NANO LETTERS

Letter

pubs.acs.org/NanoLett

Intrinsic Electronic Transport Properties of High-Quality Monolayer and Bilayer MoS_2

Britton W. H. Baugher,* Hugh O. H. Churchill, Yafang Yang, and Pablo Jarillo-Herrero*

Department of Physics, Massachusetts Institute of Technology, 77 Massachusetts Avenue, Cambridge, Massachusetts 02139, United States

Supporting Information

ABSTRACT: We report electronic transport measurements of devices based on monolayers and bilayers of the transition-metal dichalcogenide MoS_2. Through a combination of in situ vacuum annealing and electrostatic gating we obtained ohmic contact to the MoS_2 down to 4 K at high carrier densities. At lower carrier densities, low-temperature four probe transport measurements show a metal−insulator transition in both monolayer and bilayer samples. In the metallic regime, the high-temperature behavior of the mobility showed strong temperature dependence consistent with phonon-dominated transport. At low temperature, intrinsic field-effect mobilities approaching 1000 $cm^2/(V{\cdot}s)$ were observed for both monolayer and bilayer devices. Mobilities extracted from Hall effect measurements were several times lower and showed a strong dependence on density, likely caused by screening of charged impurity scattering at higher densities.

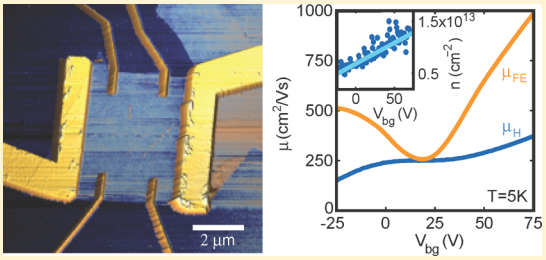

KEYWORDS: *Molybdenum disulfide (MoS2), transition metal dichalcogenides (TMD), two-dimensional (2D) electronics, layered semiconductor, contact, mobility*

Molybdenum disulfide (MoS_2), a layered transition-metal dichalcogenide (TMD) semiconductor, is attracting increasing interest for its novel nanoelectronic and optoelectronic properties.[1] Bulk MoS_2 is a stack of atomic trilayers composed of a single atomic layer of molybdenum between two layers of sulfur (Figure 1a). Strong intralayer covalent bonds lead to high mechanical strength in plane,[2] while weak van der Waals bonds between layers render the material chemically inert with robust electrical properties.[3] As with graphite, this weak interlayer coupling also allows individual layers to be isolated and studied.[4] Monolayer MoS_2 (one S−Mo−S unit) is of particular interest as a large (1.8 eV), direct-gap semiconductor[5] with strong spin−orbit interaction leading to a spin- and valley-split valence band.[6,7] These qualities could lead to novel physics such as an unconventional quantum Hall effect, combined spin Hall and valley Hall effects,[8] and new devices such as high-performance, ultralow power transistors,[9] and devices integrating spin- and valley-tronics.[10] Further, MoS_2 is compatible with standard semiconductor manufacturing,[1] can be grown in large-scale by chemical vapor deposition,[11−13] and integrated with other two-dimensional, flexible, and transparent materials.[10]

Few-layer MoS_2-based devices in field-effect transistor geometries have demonstrated the promise of these materials.[1,14−18] However, in a two-terminal contact configuration mobilities are underestimated by including contact resistance. This point is illustrated by measurements of multiterminal devices based on thick MoS_2 with mobilities up to ∼500 $cm^2/(V{\cdot}s)$, whereas two-terminal measurements showed mobilities on the order of 10−50 $cm^2/(V{\cdot}s)$.[3,19−22] Encapsulating monolayer MoS_2 in high-k dielectric or a polymer electrolyte improved device performance in several ways: increasing mobilities for monolayer devices from ∼15 $cm^2/(V{\cdot}s)$ up to ∼160 $cm^2/(V{\cdot}s)$,[10,14,23−26] increasing the on/off current ratio to 10^8 (ref 9), and enabling observation of a metal−insulator transition.[26] Nevertheless, investigation of the novel quantum transport phenomena expected for TMDs will require further improvements in device quality. Here we report multiterminal devices based on monolayer and bilayer MoS_2 with sufficiently transparent contacts at high density to enable access to the intrinsic mobility of MoS_2 at low temperatures. These measurements highlight the potential for observing novel quantum transport phenomena in TMDs.

Devices based on monolayer and bilayer MoS_2 were fabricated from bulk MoS_2 (SPI Supplies) that was exfoliated on highly doped silicon substrates with 285 nm of thermal oxide using the micromechanical cleavage process standard for graphene.[27] Monolayer and bilayer flakes were identified by optical contrast[28] and confirmed with AFM measurements (Supporting Information). We present data from two monolayer and two bilayer devices, denoted *M*1, *M*2, *B*1, and *B*2. Device contacts were patterned using PMMA masks and e-beam lithography. To optimize fabrication procedures, we investigated a number of process variations. Titanium/gold

Received: May 24, 2013
Revised: August 6, 2013
Published: August 9, 2013

   dx.doi.org/10.1021/nl401916s | *Nano Lett.* 2013, 13, 4212−4216

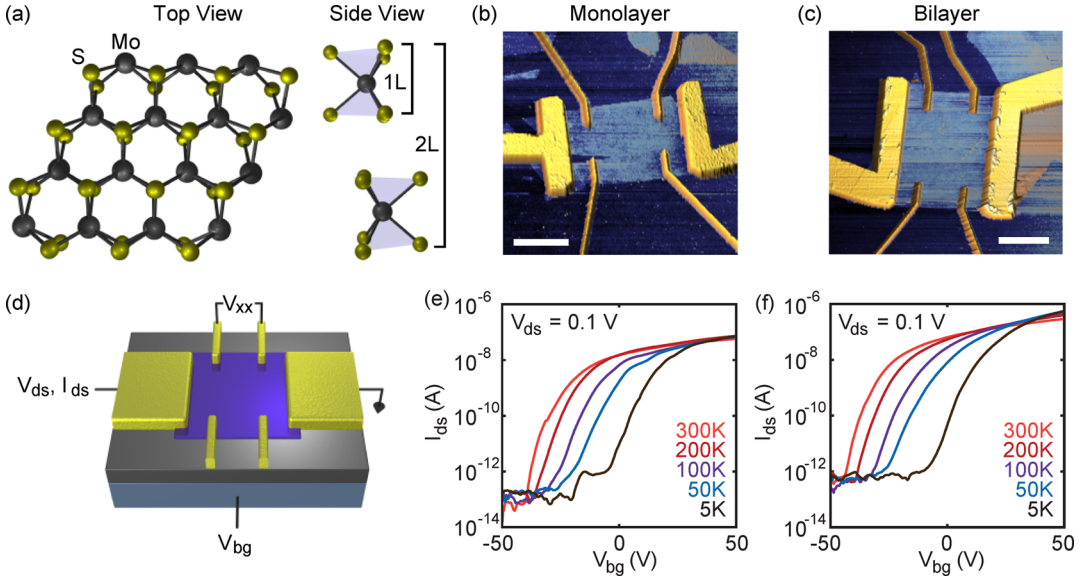

Figure 1. MoS_2 device schematics, images, and two-terminal transport measurements. (a) Structure of a single sheet of MoS_2 from both a top and side view, showing the locations of molybdenum (black) and sulfur (yellow) atoms. (b,c) Color-enhanced AFM height images of six-terminal monolayer (*M*1) and bilayer (*B*1) devices. Scale bars are 2 μm. (d) Device schematic and measurement setup. (e) Two-terminal drain-source current, I_{ds}, of monolayer MoS_2 as a function of back-gate voltage, V_{bg}. Temperatures from 300 to 5 K are denoted with traces colored from red to black in (e) and (f). (f) I_{ds} of bilayer MoS_2 as a function of V_{bg}. The dc drain-source voltage, V_{ds}, was 0.1 V for both (e) and (f). Data in (e) and (f) from devices *M*1 and *B*1.

contact metal was evaporated in thicknesses of 0.3−4 nm for Ti and 50−100 nm for Au. Some devices were annealed in an Ar/H_2 atmosphere at 350 °C for 3 hours, both before and after contacting. All of the devices were annealed in situ at high temperatures (∼120 °C) for up to 20 h in vacuum (∼10^{-6} mbar) before measurement. Variations in contact metal thickness and whether devices were annealed in Ar/H_2 were not found to have a substantial effect on mobility or contact resistance. In contrast, vacuum annealing caused a substantial drop in two-terminal resistivity (Supporting Information) and the nearly complete elimination of Schottky behavior in the contacts, even at 4 K (Figure 2).

Vacuum annealing substantially doped the sample with n-type carriers, shifting the threshold gate-voltage for conductance by as much as 100 V toward negative values. The formation of S vacancy donors would cause n-doping,[29] but this scenario is unlikely given the thermal stability of MoS_2 up to 1000 °C in vacuum.[30] We speculate that this effect points to intrinsic doping of mined, natural MoS_2.[31] The result is a large increase in carrier density and conductivity, and a significant decrease in contact resistance. After vacuum annealing, both monolayer and bilayer devices displayed stable, smooth field-effect transistor characteristics with on/off current ratios up to 10^6 (Figure 1). Two-terminal measurements such as these reiterate the viability of MoS_2 as a transistor material, but contact resistance ultimately obscures the intrinsic material properties.

To investigate the intrinsic properties of MoS_2, we further annealed our devices to reduce contact resistance, allowing us to use standard voltage-biased lockin techniques (17.78 Hz and 100 mV excitation) to measure four-probe resistivity for a second set of monolayer and bilayer devices. Without vacuum annealing, two-terminal $I-V$ measurements showed evidence of large Schottky barriers. After sufficient annealing, two-terminal $I-V$ measurements remain nearly linear at small drain-source bias, low back-gate voltage, and low temperature with a clear positive slope across zero bias at 5 K and 0 V_{bg} (insets to Figure 2a,b). Nonlinearities indicating small residual Schottky barriers begin to appear at 0 V_{bg} but are small enough to allow reliable four-terminal measurements of resistivity in the regimes studied here.

To measure the contact resistance, the devices were connected as shown in Figure 1 with the outer contacts serving as the current drain and source and two inner contacts as voltage probes. These measurements, combined with the two-probe measurements like those shown in Figure 1, allowed for the separation of the MoS_2 resistivity and the device contact resistance (both shown in Figure 2). Contact resistance was calculated from the resistivity as $R_c = V_{ds}/I_{ds} - \rho(l/w)$, where l and w are the full sample length and width, respectively, and $\rho = (V_{xx}/I_{ds})\cdot(l_{in}/w)$, with l_{in} the length between the inner contacts. Even after annealing, contact resistance makes up a significant portion of the total device resistance. Contact resistances of 5−50 kΩ could be reliably achieved at higher densities, though R_c increases to greater than 1 MΩ at low temperature and low density (Figure 2).

The temperature dependence of the resistivity provides useful information such as whether a sample is metallic or insulating and provides a means of distinguishing mobility-limiting scattering mechanisms. At high gate voltages, ρ monotonically decreases with decreasing temperature, showing a consistent metallic state for both monolayer and bilayer MoS_2 (Figure 2). In an intermediate range, ρ is nonmonotonic but ultimately increases at low temperature. At the lowest gate voltages, ρ monotonically increases with temperature, characteristic of insulating behavior. These observations indicate the presence of a metal−insulator transition in the samples with critical resistivities $\rho = 0.8\ h/e^2$ for the monolayer sample and $0.3\ h/e^2$ for the bilayer, consistent with previous observations for monolayer MoS_2[26] and theoretical expectations.[32] Other monolayer and bilayer samples we measured also showed critical resistivities of order h/e^2 (Supporting Information).

dx.doi.org/10.1021/nl401916s | *Nano Lett.* 2013, 13, 4212−4216

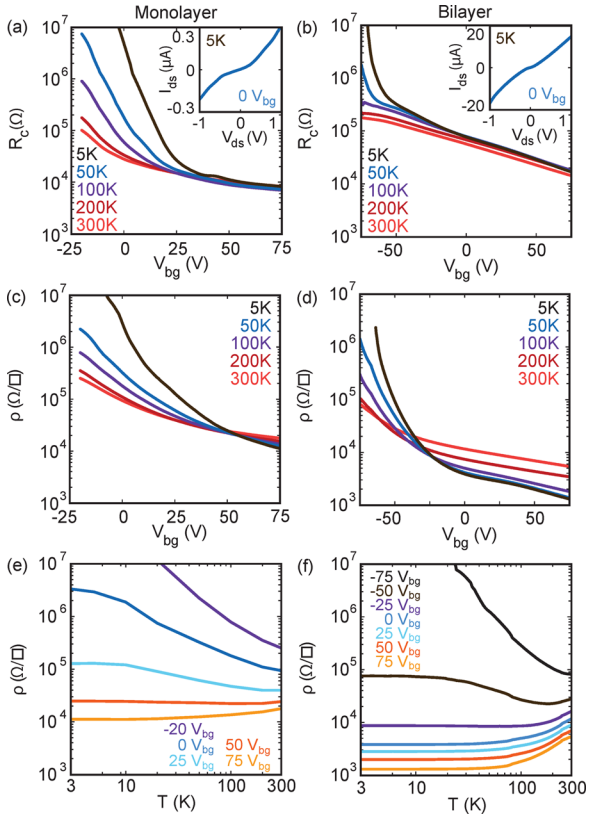

Figure 2. Contact resistance and four-terminal resistivity of monolayer and bilayer MoS_2. (a) Contact resistance, R_c, to monolayer MoS_2 as a function of V_{bg}. Curves colored from red to black show measurements at 300, 200, 100, 50, and 5 K, respectively, across panels (a–d). Inset: Two-terminal I_{ds} vs V_{ds} at 5 K and V_{bg} = 0 V for the monolayer. (b) Contact resistance, R_c, to bilayer MoS_2 as a function of V_{bg}. Inset: Two-terminal I_{ds} vs V_{ds} at 5 K and V_{bg} = 0 V for the bilayer. (c) Four-terminal resistivity of a monolayer device as a function of V_{bg}. (d) Four-terminal resistivity of a bilayer device as a function of V_{bg}. (e) Resistivity of a monolayer device as a function of temperature. The curves, from purple to yellow, correspond to V_{bg} = −20, 0, 25, 50, and 75 V. (f) Resistivity of a bilayer device as a function of temperature. The curves, from black to yellow, correspond to V_{bg} = −75, −50, −25, 0, 25, 50, and 75 V. Data from devices *M*2 and *B*2.

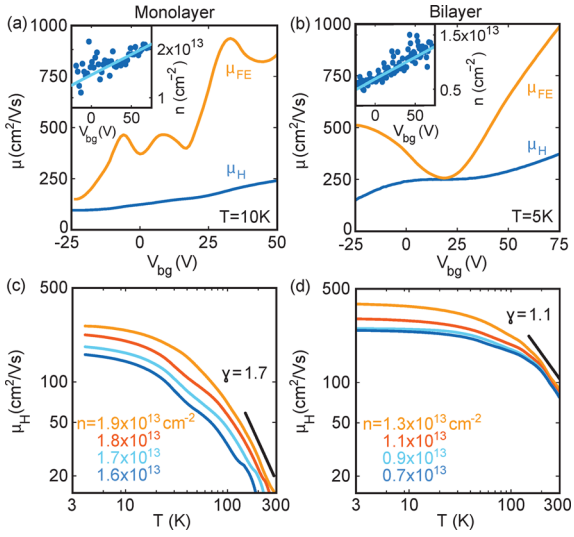

Figure 3. Field-effect and Hall mobilities as a function of back-gate voltage and temperature for monolayer and bilayer MoS_2. (a) Field-effect mobility, μ_{FE}, (yellow) and Hall mobility, μ_H, (blue) of a monolayer device as a function of back-gate voltage, V_{bg}, at 10 K. Inset: Density of a monolayer device as a function of V_{bg} at 10 K. Solid lines in the insets to (a) and (b) are fits to $n = mV_{bg} + b$, where the slope, m, and the intercept, b, are free parameters. (b) μ_{FE} (yellow) and μ_H (blue) of a bilayer device as a function of V_{bg} at 5 K. Inset: Density of a bilayer device as a function of V_{bg} at 5 K. (c) μ_H as a function of temperature for a monolayer device. The curves, from blue to yellow, correspond to n = 1.6, 1.7, 1.8, and 1.9 × 10^{13} cm^{-2}. The black line is a power law fit, $\mu_H \propto T^{-\gamma}$, with γ = 1.7 for the high density data from 150 to 300 K. (d) μ_H as a function of temperature for a bilayer device. The curves, from blue to yellow, correspond to n = 0.7, 0.9, 1.1, and 1.3 × 10^{13} cm^{-2}. The black line is a power law fit, $\mu_H \propto T^{-\gamma}$, with γ = 1.1 for the high density data from 150 to 300 K. Data from devices *M*1 and *B*2.

Hall effect measurements were used to determine carrier density, n, as a function of V_{bg}. The Hall coefficient, $R_H = 1/ne$, was calculated by fitting the slope of the transverse resistance, R_{xy}, as a function of magnetic field up to 1 T (Supporting Information). We note here that for the full gate voltage and temperature ranges of the Hall measurements, contact resistances of both the monolayer, *M*1, (with further annealing relative to data shown in Figure 1) and bilayer, *B*2, devices remained below 500 kΩ. The nearly linear dependence of n on V_{bg} corresponds to a capacitance per unit area of c = 10 ± 2 nF/cm^2 for the monolayer and 13 ± 1 nF/cm^2 for the bilayer sample (Figure 3a, b, insets). These values are in rough agreement with the capacitance expected for a parallel plate geometry, 12 nF/cm^2, which we expect to underestimate the true capacitance by about 10% due to finite size effects for an MoS_2 flake only a few times wider than the oxide thickness due to the contribution from fringing fields.[33,34] At fixed V_{bg}, the density varied with temperature significantly for the monolayer, though not for the bilayer. The monolayer density decreased by a factor of 1.5 from 300 to 5 K, whereas the density change in the bilayer was negligible (Supporting Information). A reduction in density is expected in inhomogeneous samples due to localization of charge carriers at low temperatures. Inhomogeneities in electric potential from different sources such as the substrate, charged impurities, or defects will trap more charge carriers as the device cools and the ability of carriers to be thermally excited out of these potential wells decreases.

Combining the measurements of n and ρ (*M*1's ρ can be found in the Supporting Information), we extract Hall mobility $\mu_H = \sigma/ne$ as a function of n, where $\sigma = 1/\rho$ is the conductivity and e is the electron charge (Figure 3a,b). The Hall mobilities increased with density, reaching 250 $cm^2/(V{\cdot}s)$ for the monolayer and 375 $cm^2/(V{\cdot}s)$ for the bilayer at high n. Another method commonly used to estimate carrier mobility is to calculate the field-effect mobility $\mu_{FE} = d\sigma/dV_{bg}(1/c)$, where $c = \varepsilon_r\varepsilon_0/d$ is the gate capacitance per unit area (12 nF/cm^2 for 285 nm of SiO_2). The large carrier density of these highly doped samples leads to very high field effect mobilities. Both devices show $\mu_{FE} \approx$ 1000 $cm^2/(V{\cdot}s)$ (Figure 3a,b), the highest field-effect mobilities reported to date for either monolayer or bilayer MoS_2. Encapsulating MoS_2 in a high-k dielectric has shown substantial mobility improvements.[10,14,23−26] The devices reported here are not in a high-k environment, however, suggesting the possibility of further mobility improvement in future devices.

The discrepancy between μ_H and μ_{FE} evident in Figure 3a,b can be explained by the density dependence of the Hall mobility. Substituting $\sigma = ne\mu_H$ and $ne = cV_{bg}$ into the field

dx.doi.org/10.1021/nl401916s | *Nano Lett.* 2013, 13, 4212−4216

effect mobility formula, we find $\mu_{FE} = (d/dn)(\mu_H n) = \mu_H + nd\mu_H/dn$. Thus, the field effect mobility can differ significantly from the Hall mobility if the Hall mobility changes with density. Within this model a linear trend of μ_H with density would lead to a field effect mobility trend with twice the slope (Supporting Information). Conversely, when $d\mu_H/dn$ approaches zero, the two mobility values should nearly match. These two behaviors roughly match the data: in the gate range where μ_H is nearly independent of density, μ_{FE} approaches μ_H (Figure 3b). Also, where μ_H increases with density, μ_{FE} does so at about twice the rate. Additionally, we note that the devices were not operated in a regime of saturated current with drain-source bias, a situation which would lead to a similar overestimation in the calculation of μ_{FE}.

For high densities in the metallic regime, Hall mobilities at constant density increase monotonically from 300 to 5 K for both the monolayer and the bilayer samples (Figure 3c,d). At high temperatures (above ~100 K), μ_H approximately follows a power law in temperature, $\mu_H \propto T^{-\gamma}$ with $\gamma = 1.7$ for the monolayer device and 1.1 for the bilayer. It is expected that MoS_2 devices with mobilities limited by homopolar, optical phonons should follow this form in this temperature range, with $\gamma = 1.69$ for monolayer[35] and $\gamma = 2.6$ for bulk MoS_2.[36] The monolayer value agrees well with the prediction, though we note that the fit was obtained over a limited temperature range. The power law for the bilayer sample is significantly lower than the prediction. This is similar to a previously reported value where a suppressed $\gamma = 1.4$ was attributed to phonon quenching by a top-gate dielectric.[26] Such quenching, however, is not expected in our case.

The monolayer and bilayer mobilities begin to saturate below 100 K, a temperature by which scattering from optical phonons is expected to become negligible.[35] At lower temperatures, scattering from phonons should be dominated by acoustic modes with a linear dependence of mobility on temperature,[36] in contrast with the near saturation we observe (Figure 3c,d). Another candidate explanation is mobility limited by long-range Coulomb scattering. This picture is consistent with our observation of μ_H being roughly linear with carrier density,[37] which is not expected for phonon scattering.[35] Whether the temperature dependence we observed can be mostly described by long-range Coulomb scattering awaits further experimental and theoretical study.

In conclusion, we have demonstrated high quality MoS_2 devices that may open opportunities for measuring novel quantum transport phenomena at low temperature. We showed that in situ vacuum annealing can dope devices and significantly reduce Schottky barriers and contact resistance, allowing for ohmic contact to MoS_2 down to 4 K at high densities. A clear metal–insulator transition was evident in both monolayer and bilayer samples at $\rho \sim h/e^2$, showing that high density MoS_2 devices remain conducting at low temperature. Additionally, the field-effect mobilities were quite high, indicating good sample quality. Finally, Hall mobilities calculated from density measurements gave relatively high values, though the field effect equivalents are still several times larger due to the density dependence of the Hall mobility. On the basis of the temperature and density dependence of the mobilities, we infer a crossover from a regime limited by optical phonon scattering at high temperature to one likely limited by long-range Coulomb scattering below 100 K.

■ ASSOCIATED CONTENT

Supporting Information

Supporting text and figures. This material is available free of charge via the Internet at http://pubs.acs.org.

■ AUTHOR INFORMATION

Corresponding Author

*E-mail: (B.W.H.B.) bwhb@mit.edu; (P.J.-H.) pjarillo@mit.edu.

Notes

The authors declare no competing financial interest.

■ ACKNOWLEDGMENTS

The authors would like to thank Lili Yu and Han Wang for their help with early device fabrication and measurements, and Andrea Young for many fruitful discussions. This work was funded by the ONR GATE MURI and a Packard Fellowship. This work made use of the MRSEC Shared Experimental Facilities supported by NSF under award No. DMR-0819762 and of Harvard's CNS, supported by NSF under Grant ECS-0335765.

■ REFERENCES

(1) Wang, Q. H.; Kalantar-Zadeh, K.; Kis, A.; Coleman, J. N. *Nat. Nanotechnol.* **2012**, *7*, 699.
(2) Bertolazzi, S.; Brivio, J.; Kis, A. *ACS Nano* **2011**, *5*, 9703–9709.
(3) Podzorov, V.; Gershenson, M. E.; Kloc, C.; Zeis, R.; Bucher, E. *Appl. Phys. Lett.* **2004**, *84*, 3301.
(4) Novoselov, K. S.; Jiang, D.; Booth, T.; Khotkevich, V. V.; Morozov, S. M.; Geim, A. K. *Proc. Natl. Acad. Sci. U.S.A.* **2005**, *102*, 10451.
(5) Mak, K. F.; Lee, C.; Hone, J.; Shan, J.; Heinz, T. F. *Phys. Rev. Lett.* **2010**, *105*, 136805.
(6) Evans, B. L.; Young, P. A. *Proc. R. Soc. London, Ser. A* **1965**, *284*, 402.
(7) Wilson, J. A.; Yoffe, A. D. *Adv. Phys.* **1969**, *18*, 193–335.
(8) Xiao, D.; Liu, G. B.; Feng, W.; Xu, X.; Yao, W. *Phys. Rev. Lett.* **2012**, *108*, 196802.
(9) Wang, H.; Yu, L.; Lee, Y.-H.; Fang, W.; Hsu, A.; Herring, P.; Chin, M.; Dubey, M.; Li, L.-J.; Kong, J.; Palacios, T. 2013, arXiv:1302.4027; accessed March 20, 2013.
(10) Wang, H.; Yu, L.; Lee, Y.-H.; Shi, Y.; Hsu, A.; Chin, M. L.; Li, L.-J.; Dubey, M.; Kong, J.; Palacios, T. *Nano Lett.* **2012**, *12*, 4674–4680.
(11) Lee, Y. H.; Zhang, X. Q.; Zhang, W.; Chang, M. T.; Lin, C. T.; Chang, K. D.; Yu, Y. C.; Wang, J. T. W.; Chang, C. S.; Li, L. J. *Adv. Mater.* **2012**, *24*, 2320.
(12) Liu, K.-K.; Zhang, W.; Lee, Y.-H.; Lin, Y.-C.; Chang, M.-T.; Su, C.-Y.; Chang, C.-S.; Li, H.; Shi, Y.; Zhang, H.; Lai, C.-S.; Li, L.-J. *Nano Lett.* **2012**, *12*, 1538–1544.
(13) Zhan, Y.; Liu, Z.; Najmaei, S.; Ajayan, P. M.; Lou, J. *Small* **2012**, *8*, 966.
(14) Radisavljevic, B.; Radenovic, A.; Brivio, J.; Giacometti, V.; Kis, A. *Nat. Nanotechnol.* **2011**, *6*, 147–150.
(15) Ghatak, S.; Pal, A. N.; Ghosh, A. *ACS Nano* **2011**, *5*, 7707–7712.
(16) Newaz, A. K. M.; Prasai, D.; Ziegler, J. I.; Caudel, D.; Robinson, S.; Haglund Jr, R. F.; Bolotin, K. I. 2012, arXiv:1211.0341; accessed March 20, 2013.
(17) Qiu, H.; Pan, L.; Yao, Z.; Li, J.; Shi, Y.; Wang, X. *Appl. Phys. Lett.* **2012**, *100*, 123104.
(18) Laskar, M. R.; Ma, L.; K, S.; Park, P. S.; Krishnamoorthy, S.; Nath, D. N.; Lu, W.; Wu, Y.; Rajan, S. 2013, arXiv:1302.3177; accessed April 1, 2013.
(19) Ayari, A.; Cobas, E.; Ogundadegbe, O.; Fuhrer, M. S. *J. Appl. Phys.* **2007**, *101*, 014507.

(20) Zhang, Y.; Ye, J.; Matsuhashi, Y.; Iwasa, Y. *Nano Lett.* **2012**, *12*, 1136−1140.
(21) Bao, W.; Cai, X.; Kim, D.; Sridhara, K.; Fuhrer, M. S. 2012, arXiv:1212.6292; accessed March 20, 2013.
(22) Pradhan, N. R.; Rhodes, D.; Zhang, Q.; Talapatra, S.; Terrones, M.; Ajayan, P. M.; Balicas, L. 2013, arXiv:1301.2813; accessed March 2, 2013.
(23) Liu, H.; Ye, P. D. *IEEE Electron Device Lett.* **2012**, *33*, 546−548.
(24) Lee, H. S.; Min, S.-W.; Chang, Y.-G.; Park, M. K.; Nam, T.; Kim, H.; Kim, J. H.; Ryu, S.; Im, S. *Nano Lett.* **2012**, *12*, 3695−3700.
(25) Lin, M. W.; Liu, L.; Lan, Q.; Tan, X.; Dhindsa, K. S.; Zeng, P.; Naik, V. M.; Cheng, M. M. C.; Zhou, Z. *J. Phys. D: Appl. Phys.* **2012**, *45*, 345102.
(26) Radisavljevic, B.; Kis, A. 2013, arXiv:1301.4947; accessed March 15, 2013.
(27) Novoselov, K. S.; Geim, A. K.; Morozov, S. V.; Jiang, D.; Zhang, Y.; Dubonos, S. V.; Grigorieva, I. V.; Firsov, A. A. *Science* **2004**, *306*, 666−669.
(28) Benameur, M. M.; Radisavljevic, B.; Heron, J. S.; Sahoo, S.; Berger, H.; Kis, A. *Nanotechnology* **2011**, *22*, 125706.
(29) Spah, R.; Elrod, U.; Luxsteiner, M.; Bucher, E.; Wagner, S. *Appl. Phys. Lett.* **1983**, *43*, 79−81.
(30) Spalvins, T. *J. Vac. Sci. Technol., A* **1987**, *5*, 212−219.
(31) Yin, Z.; Li, H.; Li, H.; Jiang, L.; Shi, Y.; Sun, Y.; Lu, G.; Zhang, Q.; Chen, X.; Zhang, H. *ACS Nano* **2012**, *6*, 74−80.
(32) Licciardello, D. C.; Thouless, D. J. *J. Phys. C: Solid State Phys.* **1975**, *8*, 4157.
(33) Chew, W. C.; A, K. J. *IEEE Trans. Microwave Theory Tech.* **1980**, *MTT-28*, 98.
(34) Purcell, E. M. *Electricity and Magnetism*, 2nd ed.; McGraw-Hill: New York, 1985.
(35) Kaasbjerg, K.; Thygesen, K. S.; Jacobsen, K. W. *Phys. Rev. B* **2012**, *85*, 115317.
(36) Fivaz, R.; Mooser, E. *Phys. Rev.* **1967**, *163*, 743.
(37) Ando, T.; Fowler, A. B.; Stern, F. *Rev. Mod. Phys.* **1982**, *54*, 437−672.